The effect of molnupiravir and nirmatrelvir on SARS-CoV-2 genome diversity in severe models of COVID-19.

Rebekah Penrice-Randal[1*†], Eleanor G. Bentley[1*], Parul Sharma[1], Adam Kirby[1], I'ah Donovan-Banfield[1,2], Anja Kipar[1,3], Daniele F. Mega[1] Chloe Bramwell[1,4], Joanne Sharp[4,5], Andrew Owen[4,5], Julian A. Hiscox[1,2,6] and James P. Stewart[1,5].

[1]Department of Infection Biology and Microbiomes, University of Liverpool, Liverpool, UK.

[2]NIHR Health Protection Research Unit in Emerging and Zoonotic Infections, Liverpool, UK.

[3]Laboratory for Animal Model Pathology, Institute of Veterinary Pathology, Vetsuisse Faculty, University of Zurich, Switzerland.

[4]Department of Pharmacology and Therapeutics, University of Liverpool, UK.

[5]Centre of Excellence in Long-acting Therapeutics (CELT), University of Liverpool, UK.

[6]A*STAR Infectious Diseases Laboratories (A*STAR ID Labs), Agency for Science, Technology and Research (A*STAR), Singapore.

*These authors contributed equally.

[†] Corresponding author: rebee@liverpool.ac.uk

Running title: Antiviral and SARS-CoV-2 genome diversity

Synopsis

Objectives. Immunocompromised individuals are susceptible to severe COVID-19 and potentially contribute to the emergence of variants with altered pathogenicity due to persistent infection. This study investigated the impact of immunosuppression on SARS-CoV-2 infection in k18-hACE2 mice and the effectiveness of antiviral treatments in this context during the first 7 days of infection.

Methods Mice were immunosuppressed using cyclophosphamide and infected with a B lineage of SARS-CoV-2. Molnupiravir and nirmatrelvir, alone and in combination, were administered and viral load and viral sequence diversity was assessed.

Results Treatment of infected but immune compromised mice with both compounds either singly or in combination resulted in decreased viral loads and pathological changes compared to untreated animals. Treatment also abrogated infection of neuronal tissue. However, no consistent changes in the viral consensus sequence were observed, except for the emergence of the S:H655Y mutation. Molnupiravir, but not nirmatrelvir or immunosuppression alone, increased the transition/transversion (Ts/Tv) ratio, representative of A>G and C>U mutations and this increase was not altered by the co-administration of nirmatrelvir with molnupiravir.

Notably, immunosuppression itself did not appear to promote the emergence of mutational characteristic of variants of concern (VOCs).

Conclusions Further investigations are warranted to fully understand the role of immunocompromised individuals in VOC development, especially by taking persistence into consideration, and to inform optimised public health strategies. It is more likely that immunodeficiency promotes viral persistence but does not necessarily lead to substantial consensus-level changes in the absence of antiviral selection pressure. Consistent with mechanisms of action, molnupiravir showed a stronger mutagenic effect than nirmatrelvir in this model.

Keywords

SARS-CoV-2, COVID-19, immunocompromised, intra-host evolution, Molnupiravir, Nirmatrelvir, Paxlovid.

Introduction

Unsurprisingly, since the start of the SARS-CoV-2 pandemic and the first deposited genome sequences, and like other coronaviruses, SARS-CoV-2 has diverged through single nucleotide polymorphism, and homologous and heterologous recombination applications resulting in insertions and deletions [1, 2]. Over the course of the pandemic changes that have dominated have resulted in increased transmissibility such as the P323L/D614G changes in early 2020 [3-5], immune-evasion [6] and altered pathogenicity [7].

Founder effects, population bottlenecks, selection pressures and behaviour have contributed to the diversification of the SARS-CoV-2 genome but also to the apparent waves of different variants. Several Variants of Concern (VOCs) have arisen that have a transmission advantage and/or potential immune evasion. Some reports have suggested that such variants may have arisen in hosts with compromised immunity and/or persistent infections, where infection leads to the generation of more diverse variants through longer viral evolution within an individual [8]. This includes a changing landscape of dominant viral genome sequence and minor genomic variants in immune compromised individuals e.g. in a patient with cancer [9]. Changes within the individual mapped to several different regions on the SARS-CoV-2 genome including the spike glycoprotein and orf8.

Complicating the picture of potential rapid and dramatic genomic change in immune compromised hosts is that similar changes can be observed in immune competent patients. This can be either as part of the dominant genomic sequence [10] or minor variant genomes [1]. Indeed, genomic variants with deletions can be identified in the minor genomic variant population of Middle East respiratory syndrome coronavirus (MERS-CoV) from patients [11] and as part of the dominant genomic sequence in camels [12, 13].

Parallels with other animal coronaviruses can be found where persistent infections are established, and this might be associated in pathogenicity; an example are feline coronavirus (FCoV) infections and feline infectious peritonitis (FIP) [14-17]. Thus, one

concern with long term persistence of SARS-CoV-2 in immune compromised patients is that new transmissible variants could emerge [8].

Three small molecule direct acting anti-virals (DAAs) have received early use authorisation for the treatment of COVID-19: remdesivir, molnupiravir (both nucleoside analogues which target viral nucleic acid synthesis) and nirmatrelvir (which targets the main viral protease). Unlike remdesivir, molnupiravir and nirmatrelvir are orally administered and thus more readily deployed for treatment in the community. Nirmatrelvir is packaged with ritonavir (as Paxlovid), this later molecule acting as a pharmacokinetic boosting agent to inhibit P450 (CYP) 3A4. However, adequate nirmatrelvir plasma concentrations can be achieved in mice without the need for ritonavir boosting. In cell culture single or combination treatment can result in decreased viral replication [18, 19] and a natural extension is that such anti-virals may be deployed as combination therapy to reduce the emergence of resistant genotypes [20]. Resistant genotypes/phenotypes have been identified in vitro for remdesivir [21]. Molnupiravir has previously been shown to enhance viral transition/transversion mutations in a phase II clinical trial [22] and a molnupiravir associated signature has been identified in circulating SARS-CoV-2 lineages since the introduction of molnupiravir in 2022 [23].

Immunocompromised patients with a SARS-CoV-2 infection are treated as a priority with anti-virals, including those compounds that generically target virus replication by causing hyper-mutation or specifically preventing the function of a viral protein critical to the life cycle of the virus. Such anti-virals may be deployed as combination therapy to reduce the emergence of resistant genotypes [20] and may be particularly relevant for patients with compromised immunity [24]. However, in the latter patients, anti-virals may decrease viral loads but enhance genomic plasticity. To investigate this, the genomic variation of SARS-CoV-2 was evaluated in an immune compromised host over the first 7 days of infection, in the absence and presence of medical countermeasures. We have developed animal models of COVID-19 to be able to assess pathogenicity of new variants and develop interventions [25-27]. An immune suppressed K18-hACE2 transgenic mouse model was used to simulate patients with severe COVID-19 [28, 29]. Two anti-virals, molnupiravir and nirmatrelvir, were evaluated either singly or in combination.

Methods

Animal infection and treatment

A UK variant of SARS-CoV-2 (hCoV-2/human/Liverpool/REMRQ0001/2020), was used as described previously [30, 31].

Animal work was approved by the local University of Liverpool Animal Welfare and Ethical Review Body and performed under UK Home Office Project Licence PP4715265. Transgenic mice carrying the human ACE2 gene under the control of the keratin 18 promoter (K18-hACE2; formally B6.Cg-Tg(K18-ACE2)2Prlmn/J) were purchased from Jackson Laboratories (France) at 8 – 10 weeks of age. Mice were maintained under SPF barrier conditions in individually ventilated cages and underwent a week of acclimatisation in these conditions prior to experimental use.

Experimental design is shown in Fig. 1 and treatment groups detailed in Table 1. Animals were randomly assigned into multiple cohorts of four animals using a random number generator. For operational reasons at high containment the treatment groups were not blinded during the experiment. Sample size was determined using prior experience of similar experiments with SARS-CoV-2. For SARS-CoV-2 infection, mice were anaesthetized lightly with isoflurane and inoculated intra-nasally with 50 µl containing 10^4 PFU SARS-CoV-2 in PBS as described previously [26]. Some cohorts of mice were immunosuppressed by treatment with cyclophosphamide (100 mg/kg) intra-peritoneally (IP) at day -4 and -1 pre-infection. Molnupiravir was made up in 10% PEG400 and 2.5% cremophor in water and used at 100 mg/kg. Nirmatrelvir was dissolved in 2% Tween 80 in 98% (v/v) of 0.5% methyl cellulose and used at 500 mg/kg. These does were chosen based on the known therapeutic range for these drugs in mice [32-35]. Both drugs were administered via the oral route one hour prior to infection and then twice daily up to 4 days post-infection via the oral (PO) route. Groups of animals were kept in the same cages during the experiment and were always weighed and treated in the same order. Mice were sacrificed at day 6 (vehicle and cyclophosphamide treated group) or 7 (all others) after infection by an overdose of pentobarbitone. Weights were recorded daily, and tissues were removed immediately for downstream processing. The right lung and nasal turbinates were frozen at -80 °C until further processing. The left lung and heads were fixed in 10%

155 neutral buffered formalin for 24-48 h and then stored in 70%. No data were excluded
156 from the analyses.
157
158 **Histology, immunohistology and morphometric analysis**
159 The fixed left lung was routinely paraffin wax embedded. Heads were sawn
160 longitudinally in the midline using a diamond saw (Exakt 300; Exakt) and the brain left
161 in the skull. Heads were gently decalcified in RDF (Biosystems) for twice 5 days, at
162 room temperature and on a shaker, then both halves paraffin wax embedded.
163 Consecutive sections (3-5 µm) were either stained with hematoxylin and eosin (HE)
164 or used for immunohistology (IH). IH was performed to detect viral antigen expression
165 using the horseradish peroxidase method and a rabbit anti-SARS-CoV nucleocapsid
166 protein (Rockland, 200-402-A50) as primary antibody, as previously described [26, 36,
167 37].
168 For morphometric analysis, the immunostained sections were scanned (NanoZoomer-
169 XR C12000; Hamamatsu, Hamamatsu City, Japan) and analysed using the software
170 program Visiopharm (Visiopharm 2020.08.1.8403; Visiopharm, Hoersholm, Denmark)
171 to quantify the area of viral antigen expression in relation to the total area (area
172 occupied by lung parenchyma) in the sections. This was used to compare the extent
173 of viral antigen expression in the lungs between the different treatment groups. A first
174 app was applied that outlined the entire lung tissue as ROI (total area). For this a
175 Decision Forest method was used and the software was trained to detect the lung
176 tissue section (total area). Once the lung section was outlined as ROI the lumen of
177 large bronchi and vessels was manually excluded from the ROI. Subsequently, a
178 second app with Decision Forest method was trained to detect viral antigen expression
179 (as brown DAB precipitate) within the ROI.
180
181 **qRT-PCR for viral load**
182 Viral loads were quantified using the GoTaq® Probe 1-Step RT-qPCR System
183 (Promega). For quantification of SARS-COV-2 the nCOV_N1 primer/probe mix from
184 the SARS-CoV-2 (2019-nCoV) CDC qPCR Probe Assay (IDT) were utilised and
185 murine 18S primers as described previously [25, 26].
186
187
188

189 **Sequencing of SARS-CoV-2**

190 Library preparation consisted of converting RNA to cDNA using LunaScript™
191 (Thermofisher), then amplified by reverse complement (RC)-PCR amplification
192 (EasySeq™ SARS-CoV-2 Whole Genome Sequencing kit, Nimagen, Netherlands).
193 This kit barcodes and ligates Illumina adapters in a single PCR reaction, with two
194 separate pools of primers (pools 1 and 2). After amplification, each amplicon library
195 was pooled 1:1 before being cleaned with AmpliClean™ beads and quantification. The
196 two pools were then added together and denatured. Finally, the denatured amplicon
197 library was loaded into the NovaSeq cartridge (2 x 150 bp run).

198

199 **Bioinformatics**

200 Supplementary Fig. S1 provides an overview of the workflow used in this study. In
201 short, raw paired end fastq files were inputted into the EasySeq pipeline to generate
202 alignment files, vcf's and consensus sequences using the NC_045512.2 SARS-CoV-
203 2 reference [38].Consensus sequences were inputted into Nextclade for lineage
204 assignment and bam files were inputted into DiversiTools
205 (https://github.com/josephhughes/DiversiTools) to assess minor variation.
206 Sequencing data was analysed as previously described and statistical analysis and
207 visualisation was performed in R [22]. Raw fastq files are available under SRA Project
208 Accession: PRJNA886870. Code for analysis and figure generation is available at
209 https://github.com/Hiscox-lab/viral-genomics-immunosupression-and-
210 countermeasures.

211

212 **Statistics**

213 Graphs were prepared and statistics performed using Prism 10 (Graphpad Inc). *P*
214 values were set at 95% confidence interval. A repeated-measures two-way ANOVA
215 (Bonferroni post-test) was used for time-courses of weight loss; log-rank (Mantel-Cox)
216 test was used for survival curve and Mann-Whitney *U* test for side-by-side
217 comparisons. All differences not specifically stated to be significant were not
218 significant ($p > 0.05$). For all figures, $*p < 0.05$.

219

Results and Discussion

Since the emergence of the Alpha VOC there has been discussion on the involvement of the immunocompromised host and the generation of variants [8, 39-43]. There are many case studies in the literature that follow SARS-CoV-2 evolution in immunocompromised hosts, however, the generation of VOCs is likely due to persistent infection as opposed to immunocompromised immune systems itself, little has been explored experimentally. In this study, mice were chemically immunocompromised with cyclophosphamide which is known to efficiently remove adaptive immunity in the form of B and T cells [44]. Additionally, therapeutic agents, molnupiravir and nirmatrelvir, were used independently and in combination to determine the effectiveness of these compounds in an immunocompromised model, and the impact of these compounds on viral sequence diversity during the first 7 days of infection.

Modelling an immunocompromised state in animal models in the context of SARS-CoV-2 is important for the consideration of countermeasures that may be utilised for humans who are considered vulnerable. Cyclophosphamide has been used previously to study the impact of immunosuppression in a hamster model [45-47], where intranasally infected hamsters with cyclophosphamide treatment before infection had prolonged weight loss and an inadequate neutralising antibody response to SARS-CoV-2. Distinct transcriptional profiles were identified between immunocompetent and immunosuppressed animals; however, the impact of antivirals or viral genome diversity was not investigated.

To investigate the frequency of genomic changes that occur in SARS-CoV-2 in the immune compromised or competent host in the presence or absence of antiviral drugs, K18-hACE2 transgenic mice were used as a model for severe SARS-CoV-2 infection in humans [48]. We have found that the pathological changes in the lungs in this model in many aspects resemble those in humans who have died of severe COVID-19 [26, 28, 29, 36, 37]. To mimic a host with compromised immunity, an experimental protocol was developed in which mice were exposed to cyclophosphamide [44] (Fig. 1, Table 1). Several anti-viral regimes in humans were simulated in the mouse model by giving a human equivalent dose of either molnupiravir (100 mg/kg), nirmatrelvir (500 mg/kg) or

both in combination. This included prophylactic followed by therapeutic treatment. Mice were infected with 10^4 PFU of SARS-CoV-2.

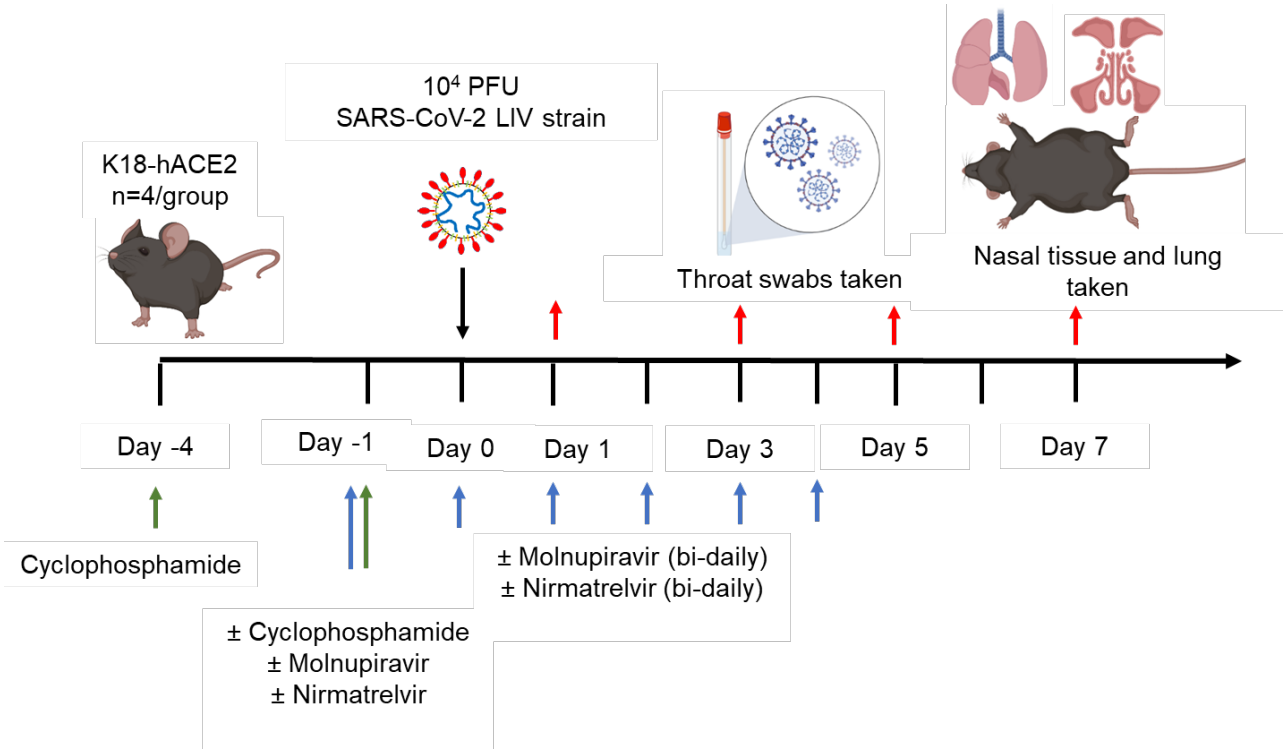

Figure 1. *Schematic diagram of the experimental design for infection of immune compromised K18-hACE2 mice with SARS-CoV-2 and evaluation of two antiviral drugs given at a human equivalent dose; molnupiravir, a broad acting compound causing error catastrophe, or nirmatrelvir which specifically targets the viral 3C-like protease. Cyclophosphamide was used at 100 mg/kg via the intraperitoneal route to immunosuppress mice. Molnupiravir was used at 100 mg/kg and* nirmatrelvir *at 500 mg/kg both via the oral route. Effects of infection and treatment were evaluated by measuring the weight of the mice daily, determining viral loads in sequential oral/throat swabs and at day 7 post-infection, and examining nose, brain and lung at day 7 post infection for any histological changes and the expression of SARS-CoV-2 nucleoprotein.*

Table 1. Treatment groups for in vivo analysis

Group	Treatment
1	Control (vehicle)
2	Cyclophosphamide
3	Molnupiravir
4	Cyclophosphamide + molnupiravir
5	Cyclophosphamide + nirmatrelvir
6	Cyclophosphamide + molnupiravir + nirmatrelvir

Treatment with Molnupiravir or Nirmatrelvir either individually or in combination provides recovery in immune compromised mice infected with SARS-CoV-2. Cyclophosphamide treatment prior to SARS-CoV-2 infection of hACE2 mice led to a more pronounced early weight loss in comparison to immunocompetent mice, a phenomenon previously reported in hamsters [47]. This was not associated with earlier mortality than in vehicle treated immunocompetent mice, although in human, a delayed adaptive immune response has been shown to be associated with fatality in COVID-19 patients, which may have been observed over longer timeframes [49]. Daily weighing of the animals indicated that all groups lost body weight after day 1 (Fig. 2). We attribute this to aversion to eating as all therapies were applied by gavage. However, starting at day 3 all groups, except for mice exposed to cyclophosphamide, or mice exposed to cyclophosphamide and treated with molnupiravir, started to gain, or stabilise weight. By days 5 and 6 a clear pattern had emerged where all groups treated with molnupiravir or nirmatrelvir either individually or in combination had regained their starting weight. The exception to this were mice exposed to vehicle only (controls) or cyclophosphamide; these reached a humane end point on day 6 (Fig. 2). Comparison of survival curves again indicated that immune compromised animals treated either singly or in combination with each therapeutic went on to survive (Fig. 3).

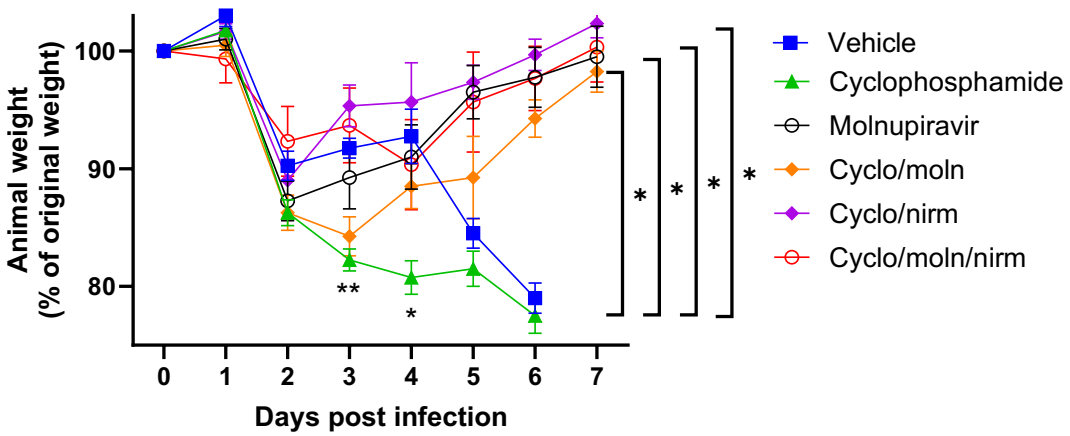

Figure 2: Treatment of SARS-CoV-2-infected mice leads to decreased weight loss. K18-hACE2 mice were challenged intranasally with 10^4 PFU SARS-CoV-2 Mice were monitored for weight at indicated time-points. (n = 4). Data represent the mean residual weight ± SEM. Comparisons were made using a repeated-measures two-way ANOVA (Bonferroni post-test). * on the represents P < 0.05. Asterisks below the curves represent * P < 0.05 and ** P < 0.01 between the cylophophamide and vehicle groups. Brackets and asterisk at the side represents P < 0.05 for the Vehicle/cycophosphamide groups and the drug treated groups.

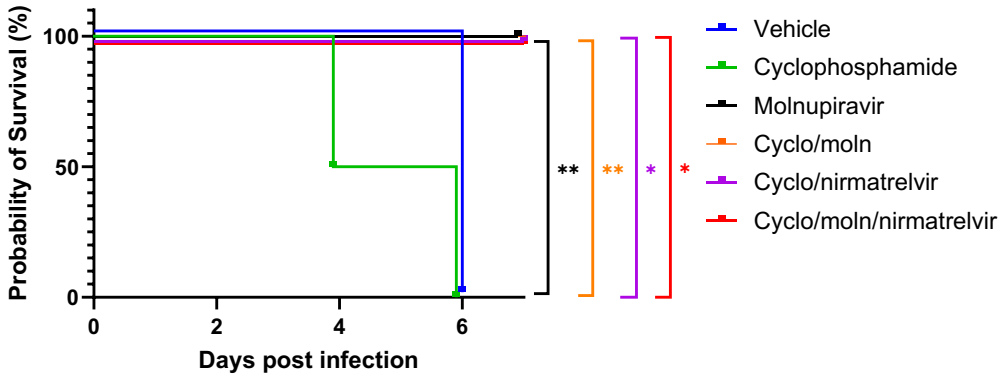

Figure 3: Treatment of SARS-CoV-2-infected mice leads to enhanced survival. *K18-hACE2 mice were challenged intranasally with 10^4 PFU SARS-CoV-2. Survival was assessed at indicated time points and significance determined using log rank (Mantel-Cox) test (n = 4).*

Viral load decreases in immune compromised mice treated with Molnupiravir or Nirmatrelvir either individually or in combination.

Viral load in terms of copy numbers of the SARS-CoV-2 genome were calculated for throat swabs during infection and compared to nasal tissue and lung tissue at the end of the experiment. The data indicated that for throat swabs on days 1 and 3 post-infection there was a significant decrease in viral load in animals treated with molnupiravir or nirmatrelvir either individually or in combination compared to untreated controls (Figure 4A). At day 3 there was a significant difference between both compounds used in combination and molnupiravir only (Figure 4A). No significant differences were observed between vehicle control and cyclophosphamide only groups.

Comparison of viral loads and titres in nasal and lung tissue respectively (Figure 4B and 4C, respectively) at day 7 post-infection reflected that there was a significantly lower viral load in animals treated with molnupiravir or nirmatrelvir either individually or in combination compared to untreated mice. However, nirmatrelvir treatment resulted in a greater decrease in viral load compared to molnupiravir. The molnupiravir/nirmatrelvir combination was also more effective at decreasing viral load than either drug alone, but this was only statistically significant in the case of molnupiravir vs the drug combination.

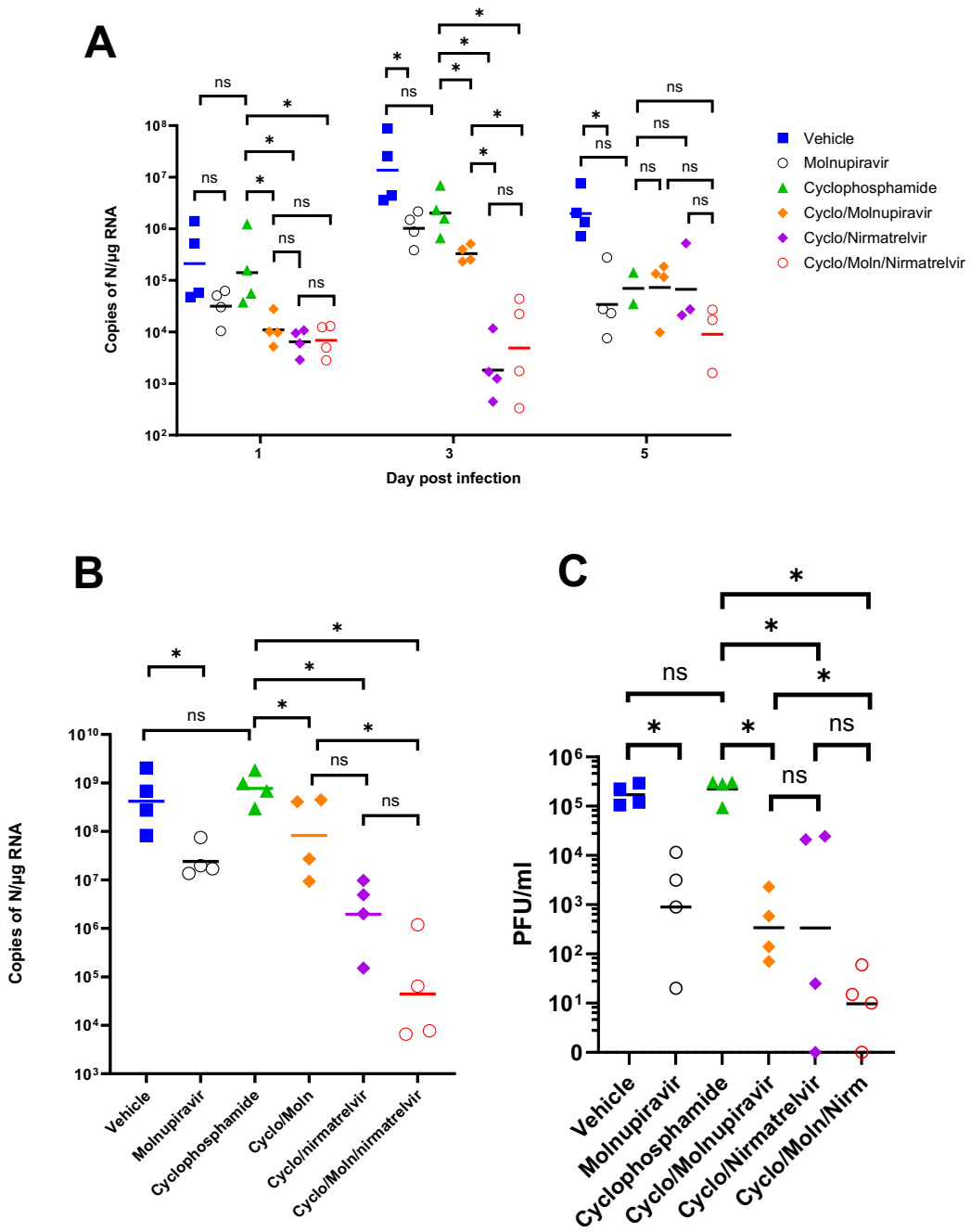

Figure 4. Viral loads in swabs and tissues. *K18-hACE2 mice were challenged intranasally with 10^4 PFU SARS-CoV-2 and treated as indicated (n = 4 per group). RNA extracted from oral/throat swabs and nasal tissue was analysed for virus RNA load using qRT-PCR and primers specific for the SARS-CoV-2 N gene. Assays were normalised relative to levels of 18S RNA. Lung tissue was analysed for live virus by plaque assay. Data for individual animals are shown with the median value represented by a black line. (A) Throat swabs; (B) nasal tissue; (C) lung tissue. Comparisons were made using two-way ANOVA (Bonferroni post-test) in panel A and Mann-Whitney U test (Panels B and C). * Represents $p < 0.05$.*

Treatment with molnupiravir or nirmatrelvir or both in combination results in marked reduction of pulmonary infection and inhibits viral spread to the brain.

The lung, nose and brain of all animals were examined for any histopathological changes and the expression of viral antigen by immunohistology, to determine whether treatment of the animals with molnupiravir and/or nirmatrelvir influenced the outcome of infection. The lungs of vehicle treated, immunocompetent animals showed the typical changes previously reported in K18-hACE2 mice infected with this virus strain [26], i.e. multifocal areas with pneumocyte degeneration, type II pneumocyte activation, mild neutrophil infiltration, and mild vasculitis, with a diffuse increase in interstitial cellularity and widespread SARS-CoV-2 antigen expression in alveolar epithelial cells (Fig. 5A). In mice that had received cyclophosphamide alone, the changes were very similar, but slightly less widespread, with some unaltered parenchyma and less extensive viral antigen expression (Fig. 5B). With molnupiravir treatment, both inflammatory processes and viral antigen expression were markedly decreased; indeed, SARS-CoV-2 antigen was only found in disseminated patches of alveoli with positive pneumocytes (Fig. 5C). With cyclophosphamide and molnupiravir treatment, the lung parenchyma was widely unaltered, and there were only small patches of inflammation and alveoli with viral antigen expression, respectively (Fig. 5D). These were further reduced in number and size in animals that had received cyclophosphamide and nirmatrelvir (Fig. 5E). Treatment with all three compounds, cyclophosphamide, molnupiravir and nirmatrelvir, resulted in widely unaltered lung parenchyma with no or minimal viral antigen expression (Fig. 5F).

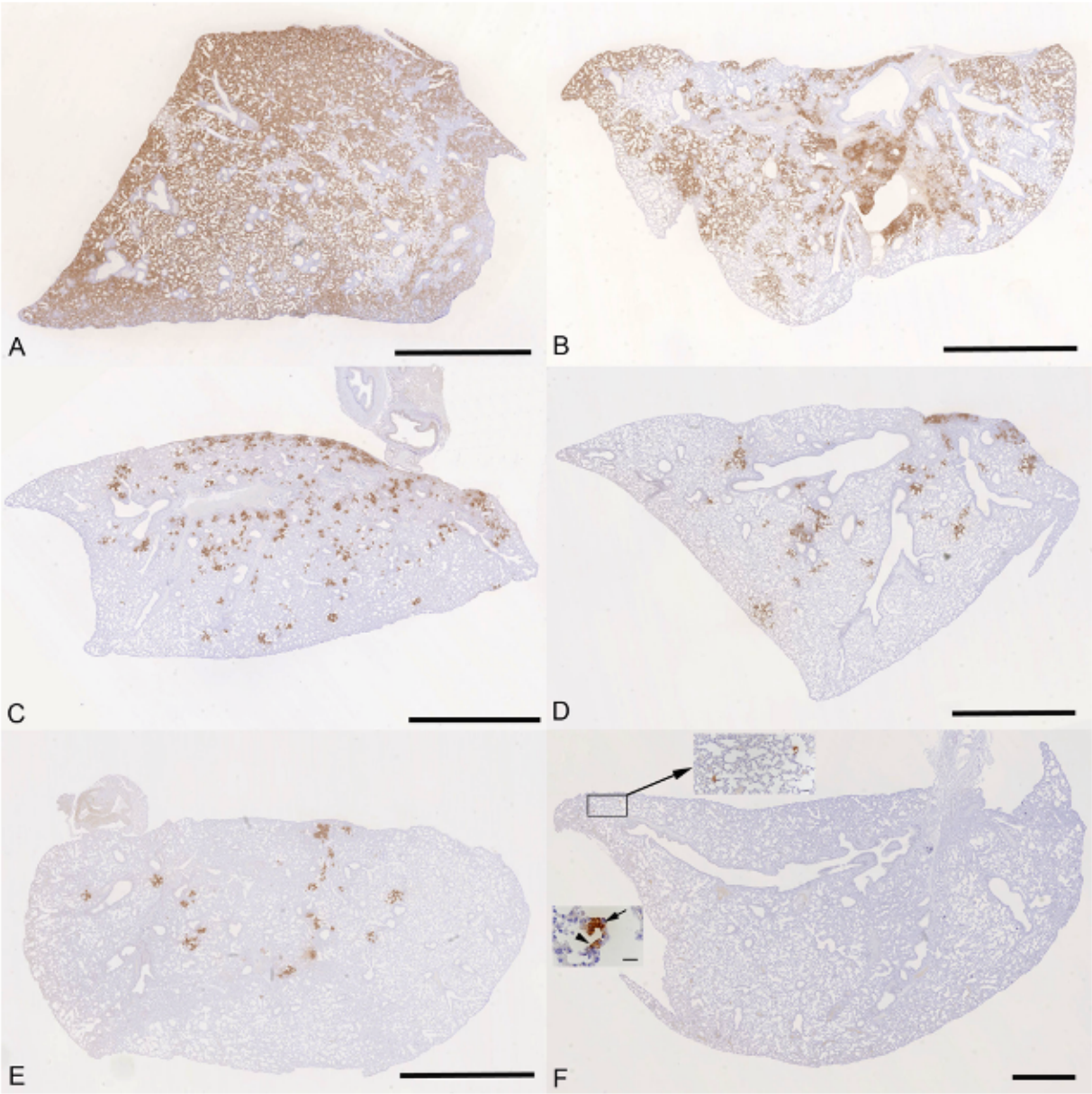

339

340 ***Figure 5****: K18-hACE2 mice were challenged intranasally with 10^4 PFU SARS-CoV-2 and*
341 *treated as indicated below (n = 4 per group). Immunohistology for the detection of viral antigen*
342 *in the lung at day 6 or 7 post infection. Sections from the formalin-fixed, paraffin embedded*
343 *left lung lobe were stained using anti-SARS-CoV nucleoprotein and counterstained with*
344 *hematoxylin. Representative images from the individual treatment groups are shown as*
345 *follows: A. vehicle; B. cyclophosphamide; C. molnupiravir; D. cyclophosphamide and*
346 *molnupiravir; E. cyclophosphamide and nirmatrelvir; F. cyclophosphamide, molnupiravir and*
347 *nirmatrelvir. Viral antigen expression is restricted to pneumocytes in a few individual alveoli*
348 *(higher magnifications in insets). Bars represent 2.5 mm (A-E), 1 mm (F) and 20 µm (F, insets).*

349 Examination of the heads using longitudinal sections (midline) revealed consistent and
350 widespread infection of the brain in animals treated with the vehicle or with
351 cyclophosphamide alone (Fig. 6A, B); this was associated with mild perivascular
352 mononuclear infiltration in particular in the brain stem, as described before in K18-
353 hACE2 mice infected with this virus strain [37]. In both groups of animals,
354 immunohistology confirmed viral antigen expression in the respiratory and/or olfactory
355 epithelium, in the latter with evidence of infection in olfactory sensory neurons (Fig.
356 6A, B). In the other groups, there was no evidence of viral infection of the brain (Fig.
357 6C-F), and viral antigen expression in the nasal mucosa was not seen or restricted to
358 scattered individual epithelial cells. In vehicle control and cyclophosphamide mice, the
359 nasal mucosa harboured viral antigen at this stage, in the respiratory epithelium and
360 in the olfactory epithelium; in the latter it also appeared to be present in sensory
361 neurons. Consequently, the virus had reached and spread widely in the brain where it
362 was detected in neurons; the infection was associated with mild inflammatory
363 response in particular in the brain stem, as described before in K18-hACE2 mice
364 infected with this virus strain [26, 37]. After treatment with all three compounds,
365 cyclophosphamide, molnupiravir and nirmatrelvir, the lung parenchyma was basically
366 unaltered, with no or minimal viral antigen expression. In all groups of mice, viral
367 antigen expression in the nasal mucosa was not seen or restricted to scattered
368 individual epithelial cells and there was no evidence of viral infection of the brain,
369 suggesting that the antiviral treatment blocked infection of the brain. Whether the latter
370 is purely a consequence of reduced viral replication in the upper respiratory tract
371 cannot be assessed in the present study; it does, however, appear likely.

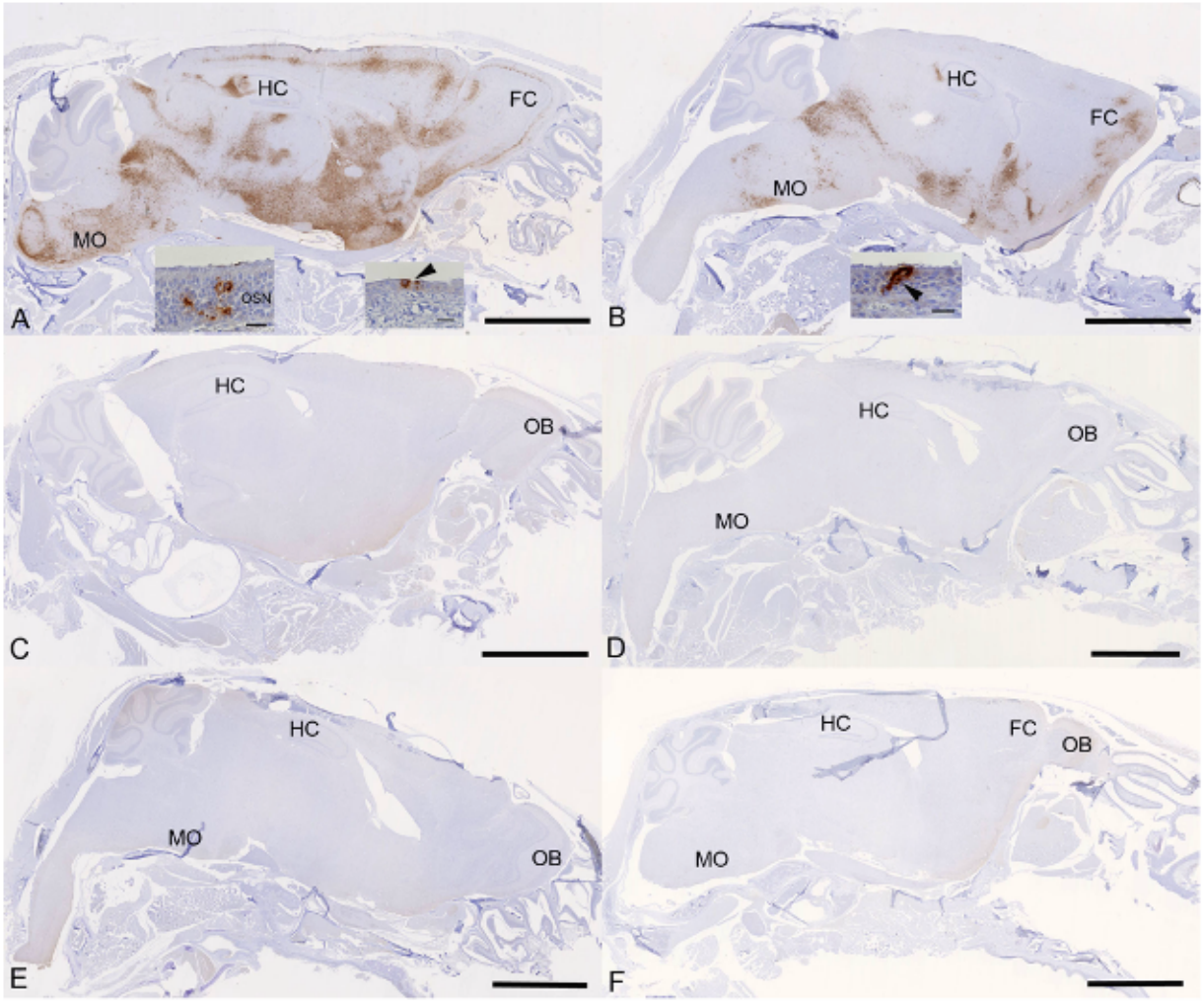

***Figure 6**: K18-hACE2 mice were challenged intranasally with 10^4 PFU SARS-CoV-2 and treated as indicated below (n = 4 per group). Immunohistology for the detection of viral antigen in the brain and nose at day 6 or 7 post infection. Sections from formalin-fixed, decalcified and paraffin embedded heads after longitudinal sawing in the midline were stained using anti-SARS-CoV nucleoprotein, and counterstained with hematoxylin. Only small fragments of nasal mucosa were available for the examination, as the nasal turbinates had been sampled for PCR. Representative images from the individual treatment groups are shown as follows: **A**. Vehicle. There is widespread infection of the brain. The insets show infection of individual cells with the morphology of olfactory sensory neurons and epithelial cells in the olfactory epithelial layer (left inset) and individual respiratory epithelial cells in the nasal mucosa (arrowhead; right inset); **B**. Cyclophosphamide. There is widespread infection of the brain. The inset shows a group of positive epithelial cells/sensory neurons in the olfactory epithelial layer (arrowhead); **C**. Molnupiravir. There is no evidence of brain infection. **D**. Cyclophosphamide and molnupiravir. There is no evidence of brain infection. **E**. Cyclophosphamide and nirmatrelvir. There is no evidence of brain infection. **F**. Cyclophosphamide, molnupiravir and nirmatrelvir. There is no evidence of brain infection. Bars represent 2.5 mm (A-F) and 20 µm (A, B insets). FC – frontal cortex, HC – hippocampus, MO – medulla oblongata, OB – olfactory bulb, OSN - olfactory sensory neurons.*

391 **Evaluation of dominant and minor variants in SARS-CoV-2**

392 To determine the impact of immunosuppression on viral diversity, 116 RNA samples
393 from swabs and tissue were sequenced and analysed using the EasySeq WGS
394 protocol by Nimagen. alignment files and associated index files were inputted into
395 DiversiTools to provide mutation data and outputs were analysed in R. Samples with
396 less than 90% breadth of coverage were discarded for mutational analysis (n=12), as
397 well as samples that returned bad or mediocre quality scores in nextclade (n=13). The
398 samples that were excluded were associated with higher Ct values and later time
399 points belonging in the nirmatrelvir treatment groups. Sequencing data from 89
400 samples were taken forward in the analysis (swab, n=50, tissue n=39, Supplementary
401 Table S1).
402
403 The input virus contained 5 substitutions and 3 amino acid substitutions in comparison
404 to the reference sequence (NC_045512.2) and were thus not considered as changes
405 during the analysis (Supplementary Table S2). The S: H655Y mutation was present in
406 76% of the genomes that passed QC at the dominant level and observed as a minor
407 variant across all samples (Supplementary Fig. S2). This mutation has been reported
408 previously as a spike adaptation to other species such as cats, hamsters, and mink [50-
409 52] and of course has independently arisen in human lineages such as Omicron [53]. As
410 this mutation was clearly associated with a species adaptation, it was disregarded for
411 the evaluation of treatment and immune status driven mutations. The other mutations
412 appear to be novel at the time of writing; however, no distinct group was associated
413 with driving these mutations, and can be overall interpreted as a rare event. The
414 sequences showing the highest number of mutations were sequences derived from
415 tissue samples. The species specific adaptation S:H655Y was observed more
416 frequently in the dataset, where there was little evidence of adaptations specific to
417 immunocompromised and antiviral environments, putting the evolutionary pressures
418 into perspective. Adaptations associated with immunosuppression and antiviral
419 treatment may emerge in the context of persistent replication of the virus which would
420 need to be investigated.
421
422
423

424 **Molnupiravir increases the Ts/Tv ratio at the minor variant level in genomes**
425 **derived from swabs**
426 To further assess the impact of immunocompromising mice by cyclophosphamide, and
427 the therapeutic agents molnupiravir and the nirmatrelvir, a minor variant analysis was
428 conducted on samples derived from throat swabs. The average transition/transversion
429 (Ts/Tv) ratio for SARS-CoV-2 genomes from each mouse and the mean of each group
430 was compared across cohorts at day 1, day 3 and day 5 of infection in line with analysis
431 performed previously in a phase II clinical trial [22]. On day 1, an increase in Ts/Tv ration
432 was observed in the molnupiravir cohort and the cyclophosphamide and molnupiravir
433 cohort and had a p value < 0.05 when compared to the vehicle control and
434 cyclophosphamide only groups (Fig. 7). The number of samples analysed for
435 cyclophosphamide and nirmatrelvir only was too small for statistical analysis, however,
436 the trend resembles that of vehicle and cyclophosphamide only with little change in
437 the Ts/Tv ratio. Likewise, the combined cyclophosphamide and molnupiravir and
438 nirmatrelvir cohort is represented by one genome derived from one mouse, due to low
439 sequencing coverage obtained from the other mice within this group, however, the
440 trend resembles that of other genomes with exposure to molnupiravir with an
441 increased Ts/Tv ratio. The same is observed at day 3 of sampling, however, there is
442 a significant difference between the mean Ts/Tv ratio between the molnupiravir only
443 and cyclophosphamide and molnupiravir groups. Importantly, the Ts/Tv ratios
444 between the vehicle control and cyclophosphamide only groups resemble each other
445 demonstrating that immunosuppression itself does not drive diversification of the viral
446 genome over this time course. The proportion of base changes were also observed,
447 with particular interest in the C to U and G to A transitions as previously seen in a
448 phase II clinical trial [22] (Figure 8).
449
450 Further investigations are warranted to understand completely the role of
451 immunocompromised individuals in the development of SARS-CoV-2 variants. It is
452 more likely that immunodeficiency promotes viral persistence providing the virus
453 more opportunity to replicate and introduce mutations. Molnupiravir, compared to
454 nirmatrelvir, shows a stronger mutagenic effect in this model at the minor variant
455 level, however, data is insufficient to make conclusions regards consensus level
456 changes over the timeframes used in this study. When these therapies are used
457 individually or in combination, there is successful depletion in viral load and animals

recover from infection, whilst preventing infiltration into brain tissue. Given the concern of molnupiravir associated lineages in circulation [23], combination therapy may reduce this through more effective clearance of the virus [20], although this would need to be evaluated over time in a real-world setting as the mutational signatures were observed in the combined therapy group.

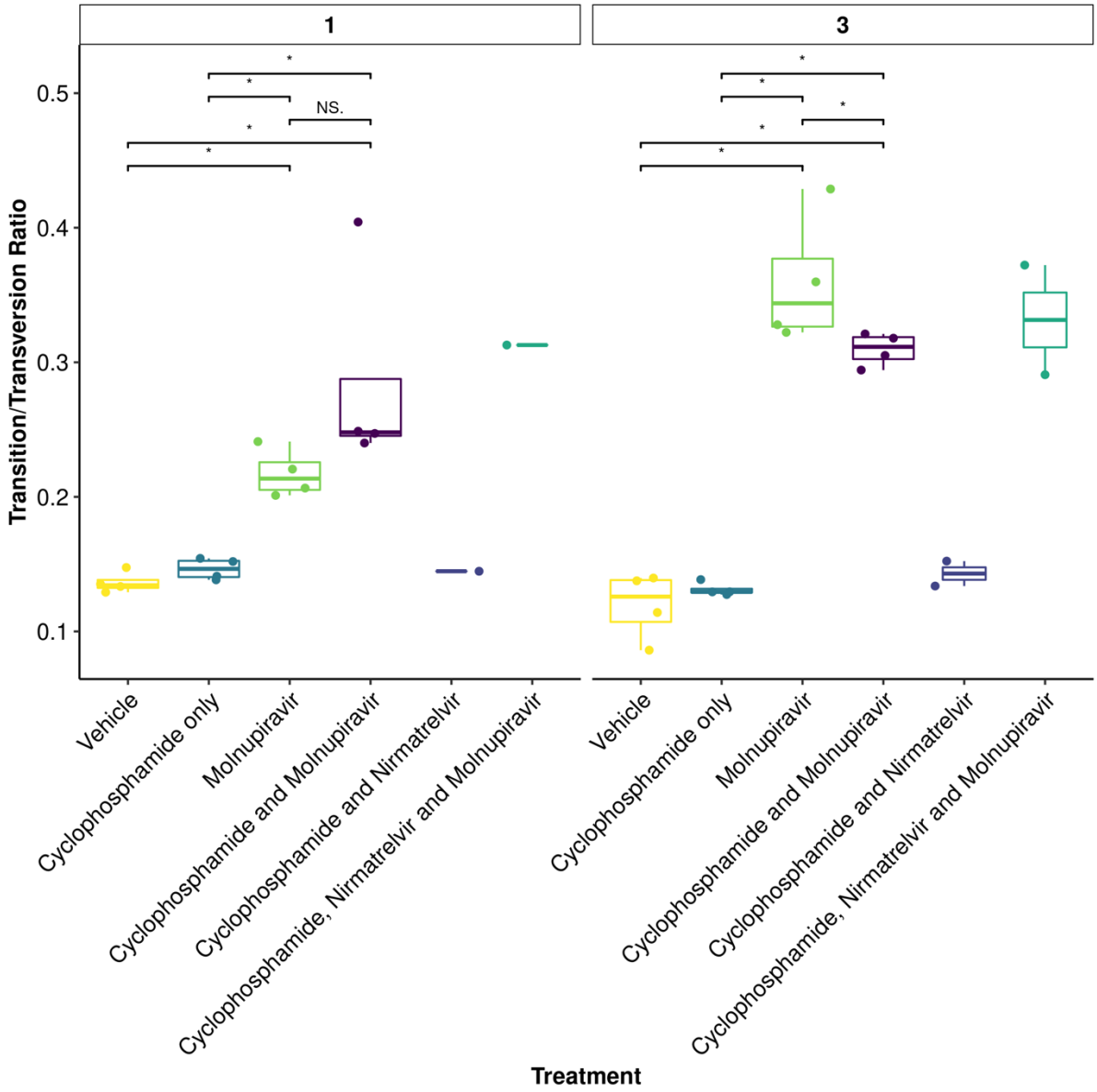

Figure 7: *The mean Ts/Tv ratio per genome plotted as boxplots. The plot is facetted by day post infection. Less genomes were recovered for cyclophosphamide and* nirmatrelvir *and cyclophosphamide,* nirmatrelvir *and molnupiravir, therefore statistical analysis returns the differences as non-significant. Trends can be concluded with caution. * Represents a P value <0.05 (Mann Whitney U test).*

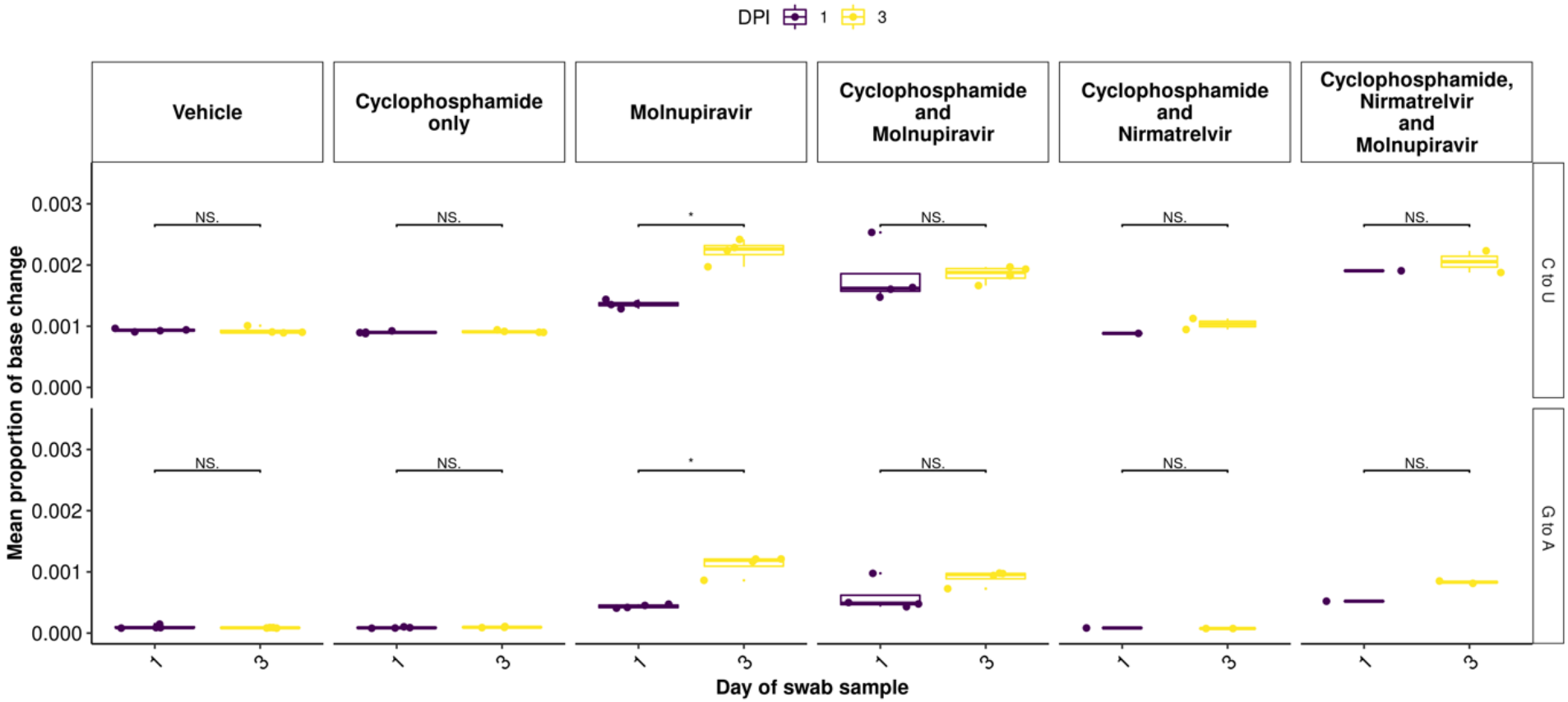

Figure 8: *C to U and G to A minor variation changes significantly increased between day 1 and day 3 post infection in the molnupiravir only group. A similar trend is observed between other groups including molnupiravir treatment, however, the change is not reported as significant. * represents a P value <0.05 (Mann Whitney U test).*

Acknowledgements

The authors are grateful to the technical staff at the Histology Laboratory, Institute of Veterinary Pathology, Vetsuisse Faculty, University of Zurich, for excellent technical support. JAH is a member of the ISARIC4C consortium (https://isaric4c.net/about/authors/), and we thank them for the use of the SARS-CoV-2 isolate used in this study.

Funding

This work was funded by the MRC (MR/W005611/1) 'G2P-UK: A national virology consortium to address phenotypic consequences of SARS-CoV-2 genomic variation' and MR/Y004205/1 'The G2P2 virology consortium: keeping pace with SARS-CoV-2 variants, providing evidence to vaccine policy, and building agility for the next pandemic' (co-Is JPS and JAH) and funded in part by U.S. Food and Drug Administration Medical Countermeasures Initiative contract (75F40120C00085) to JAH. The article reflects the views of the authors and does not represent the views or policies of the FDA. Additionally, DNDi under the support by the Wellcome Trust (Grant ref: 222489/Z/21/Z to AO and JPS) through the 'COVID-19 Therapeutics Accelerator'. A.O. acknowledges funding by Wellcome Trust (222489/Z/21/Z), EPSRC (EP/R024804/1; EP/S012265/1) and National Institute of Health (NIH) (R01AI134091; R24AI118397). J.P.S. also acknowledges funding from the Medical Research Council (MRC) (MR/R010145/1, MR/W021641/1, PA6162_G2P2-2023), BBSRC (BB/R00904X/1; BB/R018863/1; BB/N022505/1) and Innovate UK (TS/W022648/1). A.K. received support from the Swiss National Science Foundation (SNSF; IZSEZ0 213289).

Transparency Declaration

A.O. is a director of Tandem Nano Ltd and co-inventor of patents relating to drug delivery. A.O. has been co-investigator on funding received by the University of Liverpool from ViiV Healthcare and Gilead Sciences in the past 3 years unrelated to COVID-19. A.O. has received personal fees from Gilead and Assembly Biosciences in the past 3 years, also unrelated to COVID-19. JPS has received funding from ENA respiratory Pty Ltd, Bicycle Tx Ltd, and Infex Therapeutics Ltd unrelated to this study. R.P.R. is an employee at TopMD Precision Medicine Ltd. No other conflicts are declared by the authors.

504 **References**

505 1. Moore SC, Penrice-Randal R, Alruwaili M et al. Amplicon-Based Detection and
506 Sequencing of SARS-CoV-2 in Nasopharyngeal Swabs from Patients With COVID-19 and
507 Identification of Deletions in the Viral Genome That Encode Proteins Involved in Interferon
508 Antagonism. *Viruses* 2020; **12**.
509 2. McCarthy KR, Rennick LJ, Nambulli S et al. Natural deletions in the SARS-CoV-2 spike
510 glycoprotein drive antibody escape. *bioRxiv* 2020: 2020.11.19.389916.
511 3. Korber B, Fischer WM, Gnanakaran S et al. Tracking Changes in SARS-CoV-2 Spike:
512 Evidence that D614G Increases Infectivity of the COVID-19 Virus. *Cell* 2020; **182**: 812-27 e19.
513 4. Alruwaili M, Armstrong S, Prince T et al. SARS-CoV-2 NSP12 associates with TRiC and
514 the P323L substitution acts as a host adaption. *Journal of virology* 2023; **97**: e0042423.
515 5. Goldswain H, Dong X, Penrice-Randal R et al. The P323L substitution in the SARS-CoV-
516 2 polymerase (NSP12) confers a selective advantage during infection. *Genome Biology* 2023;
517 **24**: 47.
518 6. Wang B, Goh YS, Prince T et al. Resistance of SARS-CoV-2 variants to neutralization by
519 convalescent plasma from early COVID-19 outbreak in Singapore. *NPJ Vaccines* 2021; **6**: 125.
520 7. Suzuki R, Yamasoba D, Kimura I et al. Attenuated fusogenicity and pathogenicity of
521 SARS-CoV-2 Omicron variant. *Nature* 2022; **603**: 700-5.
522 8. Corey L, Beyrer C, Cohen MS et al. SARS-CoV-2 Variants in Patients with
523 Immunosuppression. *N Engl J Med* 2021; **385**: 562-6.
524 9. Avanzato VA, Matson MJ, Seifert SN et al. Case Study: Prolonged Infectious SARS-CoV-
525 2 Shedding from an Asymptomatic Immunocompromised Individual with Cancer. *Cell* 2020;
526 **183**: 1901-12 e9.
527 10. Young BE, Fong SW, Chan YH et al. Effects of a major deletion in the SARS-CoV-2
528 genome on the severity of infection and the inflammatory response: an observational cohort
529 study. *Lancet* 2020; **396**: 603-11.
530 11. Aljabr W, Alruwaili M, Penrice-Randal R et al. Amplicon and Metagenomic Analysis of
531 Middle East Respiratory Syndrome (MERS) Coronavirus and the Microbiome in Patients with
532 Severe MERS. *mSphere* 2021; **6**: e0021921.
533 12. Chu DKW, Hui KPY, Perera R et al. MERS coronaviruses from camels in Africa exhibit
534 region-dependent genetic diversity. *Proc Natl Acad Sci U S A* 2018; **115**: 3144-9.
535 13. El-Kafrawy SA, Corman VM, Tolah AM et al. Enzootic patterns of Middle East
536 respiratory syndrome coronavirus in imported African and local Arabian dromedary camels:
537 a prospective genomic study. *Lancet Planet Health* 2019; **3**: e521-e8.
538 14. Rottier PJ, Nakamura K, Schellen P et al. Acquisition of macrophage tropism during the
539 pathogenesis of feline infectious peritonitis is determined by mutations in the feline
540 coronavirus spike protein. *Journal of virology* 2005; **79**: 14122-30.
541 15. Licitra BN, Millet JK, Regan AD et al. Mutation in spike protein cleavage site and
542 pathogenesis of feline coronavirus. *Emerg Infect Dis* 2013; **19**: 1066-73.
543 16. Vennema H, Poland A, Foley J et al. Feline infectious peritonitis viruses arise by
544 mutation from endemic feline enteric coronaviruses. *Virology* 1998; **243**: 150-7.
545 17. Kipar A, Meli ML, Baptiste KE et al. Sites of feline coronavirus persistence in healthy
546 cats. *The Journal of general virology* 2010; **91**: 1698-707.
547 18. Li P, Wang Y, Lavrijsen M et al. SARS-CoV-2 Omicron variant is highly sensitive to
548 molnupiravir, nirmatrelvir, and the combination. *Cell Res* 2022; **32**: 322-4.

549 19. Gidari A, Sabbatini S, Schiaroli E et al. The Combination of Molnupiravir with
550 Nirmatrelvir or GC376 Has a Synergic Role in the Inhibition of SARS-CoV-2 Replication In Vitro.
551 *Microorganisms* 2022; **10**.
552 20. Hiscox JA, Khoo SH, Stewart JP et al. Shutting the gate before the horse has bolted: is
553 it time for a conversation about SARS-CoV-2 and antiviral drug resistance? *J Antimicrob*
554 *Chemother* 2021; **76**: 2230-3.
555 21. Szemiel AM, Merits A, Orton RJ et al. In vitro selection of Remdesivir resistance
556 suggests evolutionary predictability of SARS-CoV-2. *PLoS Pathog* 2021; **17**: e1009929.
557 22. Donovan-Banfield Ia, Penrice-Randal R, Goldswain H et al. Characterisation of SARS-
558 CoV-2 genomic variation in response to molnupiravir treatment in the AGILE Phase IIa clinical
559 trial. *Nature Communications* 2022; **13**: 7284-.
560 23. Sanderson T, Hisner R, Donovan-Banfield Ia et al. A molnupiravir-associated
561 mutational signature in global SARS-CoV-2 genomes. *Nature* 2023; **623**: 594-600.
562 24. Li P, de Vries AC, Kamar N et al. Monitoring and managing SARS-CoV-2 evolution in
563 immunocompromised populations. *Lancet Microbe* 2022; **3**: e325-e6.
564 25. Bentley EG, Kirby A, Sharma P et al. SARS-CoV-2 Omicron-B.1.1.529 Variant leads to
565 less severe disease than Pango B and Delta variants strains in a mouse model of severe COVID-
566 19. *bioRxiv* 2021: 2021.12.26.474085.
567 26. Clark JJ, Penrice-Randal R, Sharma P et al. Sequential infection with influenza A virus
568 followed by severe acute respiratory syndrome coronavirus 2 (SARS-CoV-2) leads to more
569 severe disease and encephalitis in a mouse model of COVID-19. *bioRxiv* 2023:
570 2020.10.13.334532.
571 27. Gaynor KU, Vaysburd M, Harman MAJ et al. Multivalent bicyclic peptides are an
572 effective antiviral modality that can potently inhibit SARS-CoV-2. *Nature Communications*
573 2023; **14**: 3583.
574 28. Russell CD, Valanciute A, Gachanja NN et al. Tissue Proteomic Analysis Identifies
575 Mechanisms and Stages of Immunopathology in Fatal COVID-19. *Am J Respir Cell Mol Biol*
576 2021.
577 29. Dorward DA, Russell CD, Um IH et al. Tissue-Specific Immunopathology in Fatal COVID-
578 19. *Am J Respir Crit Care Med* 2021; **203**: 192-201.
579 30. Patterson EI, Prince T, Anderson ER et al. Methods of Inactivation of SARS-CoV-2 for
580 Downstream Biological Assays. *J Infect Dis* 2020; **222**: 1462-7.
581 31. Davidson AD, Williamson MK, Lewis S et al. Characterisation of the transcriptome and
582 proteome of SARS-CoV-2 reveals a cell passage induced in-frame deletion of the furin-like
583 cleavage site from the spike glycoprotein. *Genome Med* 2020; **12**: 68.
584 32. Abdelnabi R, Foo CS, Kaptein SJF et al. A SCID Mouse Model To Evaluate the Efficacy
585 of Antivirals against SARS-CoV-2 Infection. *Journal of virology* 2022; **96**: e00758-22.
586 33. Jeong JH, Chokkakula S, Min SC et al. Combination therapy with nirmatrelvir and
587 molnupiravir improves the survival of SARS-CoV-2 infected mice. *Antiviral Research* 2022;
588 **208**: 105430.
589 34. Wahl A, Gralinski LE, Johnson CE et al. SARS-CoV-2 infection is effectively treated and
590 prevented by EIDD-2801. *Nature* 2021; **591**: 451-7.
591 35. Stegmann KM, Dickmanns A, Heinen N et al. Inhibitors of dihydroorotate
592 dehydrogenase cooperate with molnupiravir and N4-hydroxycytidine to suppress SARS-CoV-
593 2 replication. *iScience* 2022; **25**: 104293.
594 36. De Neck S, Penrice-Randal R, Clark JJ et al. The Stereotypic Response of the Pulmonary
595 Vasculature to Respiratory Viral Infections: Findings in Mouse Models of SARS-CoV-2,

596 Influenza A and Gammaherpesvirus Infections. Viruses 2023; 15(8) (Access Date Access 2023,
597 date last accessed).
598 37. Seehusen F, Clark JJ, Sharma P et al. Neuroinvasion and Neurotropism by SARS-CoV-2
599 Variants in the K18-hACE2 Mouse. *Viruses* 2022; **14**.
600 38. Coolen JPM, Wolters F, Tostmann A et al. SARS-CoV-2 whole-genome sequencing
601 using reverse complement PCR: For easy, fast and accurate outbreak and variant analysis.
602 *Journal of Clinical Virology* 2021; **144**: 104993.
603 39. Avanzato VA, Matson MJ, Seifert SN et al. Case Study: Prolonged Infectious SARS-CoV-
604 2 Shedding from an Asymptomatic Immunocompromised Individual with Cancer. *Cell* 2020;
605 **183**: 1901-12.e9.
606 40. Burki T. The origin of SARS-CoV-2 variants of concern. *Lancet Infect Dis* 2022; **22**: 174-
607 5.
608 41. Caccuri F, Messali S, Bortolotti D et al. Competition for dominance within replicating
609 quasispecies during prolonged SARS-CoV-2 infection in an immunocompromised host. *Virus*
610 *Evol* 2022; **8**: veac042.
611 42. Chen L, Zody MC, Di Germanio C et al. Emergence of Multiple SARS-CoV-2 Antibody
612 Escape Variants in an Immunocompromised Host Undergoing Convalescent Plasma
613 Treatment. *mSphere* 2021; **6**: e0048021.
614 43. Choi B, Choudhary MC, Regan J et al. Persistence and Evolution of SARS-CoV-2 in an
615 Immunocompromised Host. *New England Journal of Medicine* 2020; **383**: 2291-3.
616 44. Peng KW, Myers R, Greenslade A et al. Using clinically approved cyclophosphamide
617 regimens to control the humoral immune response to oncolytic viruses. *Gene Therapy* 2013;
618 **20**: 255-61.
619 45. Schaecher SR, Stabenow J, Oberle C et al. An immunosuppressed Syrian golden
620 hamster model for SARS-CoV infection. *Virology* 2008; **380**: 312-21.
621 46. Ramasamy S, Kolloli A, Kumar R et al. Comprehensive Analysis of Disease Pathology in
622 Immunocompetent and Immunocompromised Hosts following Pulmonary SARS-CoV-2
623 Infection. *Biomedicines* 2022; **10**: 1343.
624 47. Brocato RL, Principe LM, Kim RK et al. Disruption of Adaptive Immunity Enhances
625 Disease in SARS-CoV-2-Infected Syrian Hamsters. *J Virol* 2020; **94**.
626 48. Salzer R, Clark JJ, Vaysburd M et al. Single-dose immunisation with a multimerised
627 SARS-CoV-2 receptor binding domain (RBD) induces an enhanced and protective response in
628 mice. *FEBS Lett* 2021; **595**: 2323-40.
629 49. Legebeke J, Lord J, Penrice-Randal R et al. Evaluating the Immune Response in
630 Treatment-Naive Hospitalised Patients With Influenza and COVID-19. *Front Immunol* 2022;
631 **13**: 853265.
632 50. Escalera A, Gonzalez-Reiche AS, Aslam S et al. Mutations in SARS-CoV-2 variants of
633 concern link to increased spike cleavage and virus transmission. *Cell Host Microbe* 2022; **30**:
634 373-87.e7.
635 51. Braun KM, Moreno GK, Halfmann PJ et al. Transmission of SARS-CoV-2 in domestic
636 cats imposes a narrow bottleneck. *PLOS Pathogens* 2021; **17**: e1009373.
637 52. Mizuki Y, Keiko T, Youko H et al. SARS-CoV-2 Omicron spike H655Y mutation is
638 responsible for enhancement of the endosomal entry pathway and reduction of cell surface
639 entry pathways. *bioRxiv* 2022: 2022.03.21.485084.
640 53. Ou J, Lan W, Wu X et al. Tracking SARS-CoV-2 Omicron diverse spike gene mutations
641 identifies multiple inter-variant recombination events. *Signal Transduction and Targeted*
642 *Therapy* 2022; **7**: 138.

643 # SUPPLEMENTARY TABLES

644 ***Table S1:*** *The number of samples per cohort, sample type and DPI that were included*
645 *in the sequencing analysis. Samples with less than 90% coverage and poor or*
646 *mediocre quality control results determined by Nextclade CLI, were excluded from the*
647 *analysis. *Multiple end point time-points due to humane end-point variation.*

648

Cohort	Sample type	DPI*	*n*
Cyclophosphamide and Molnupiravir	Swab	1	4
		3	4
		5	3
	Lung Tissue	7	4
	Nasal Tissue	7	4
Cyclophosphamide and nirmatrelvir	Swab	1	1
		3	2
		5	1
	Lung Tissue	4	1
		7	2
	Nasal Tissue	4	1
		7	2
Cyclophosphamide only	Swab	1	4
		3	4
		4	1
		5	2
	Lung Tissue	4	2
		6	2
	Nasal Tissue	4	1
		6	2
Cyclophosphamide, nirmatrelvir and Molnupiravir	Swab	1	1
		3	2

Cohort	Sample type	DPI*	*n*
	Lung Tissue	3	1
		7	2
	Nasal Tissue	3	1
		7	3
Molnupiravir	Swab	1	4
		3	4
		5	1
	Lung Tissue	7	3
	Nasal Tissue	7	1
Vehicle	Swab	1	4
		3	4
		5	4
	Lung Tissue	6	4
	Nasal Tissue	6	3

649

650

651

652 **Table S2: Input virus**

653

Input virus		
Nucleotide change	**Gene**	**Amino Acid Change**
A6948C	Nsp3	N1410T or N2228T
G11083T	Nsp6	L37F or L3606F
C21005T	Nsp16	A116V or A2513V
C25452T	Orf3a	I20 no change
C28253T	Orf8	F120 no change

654

655 ***Table S3:*** *Unique phenotypic changes in SARS-CoV-2 within the dataset. Input virus*

656 *amino acids and S: H665Y were excluded.*

Amino acid change	Occurrence in dataset	Tissue type	Cohorts
S: D215H	2	Swab	Vehicle, Cyclophosphamide, Molnupiravir & nirmatrelvir
ORF1a: G2581S	1	Swab	Cyclophosphamide & nirmatrelvir
ORF3a: P42L	1	Swab	Cyclophosphamide & Molnupiravir
ORF3a: Q57H	2	Nasal Tissue Swab	Cyclophosphamide, Molnupiravir & nirmatrelvir, Cyclophosphamide only
E: Y42H	1	Swab	Cyclophosphamide & nirmatrelvir
ORF1a: G82D	1	Lung Tissue	Cyclophosphamide, nirmatrelvir and Molnupiravir
S: V47I			Cyclophosphamide, nirmatrelvir and Molnupiravir
ORF1a: T568I	1	Nasal Tissue	Cyclophosphamide, nirmatrelvir and Molnupiravir
ORF1a: C2160Y			
ORF1b: F312L			
ORF1b: V2515I			
ORF8: F108L			
S: A27T			
ORF1a: F741L	1	Nasal Tissue	Cyclophosphamide & nirmatrelvir
ORF1a: A872T			
ORF7b: S5P			

Amino acid change	Occurrence in dataset	Tissue type	Cohorts
S: A890V			
S: D985N			
ORF1a: F190L	1	Nasal Tissue	Molnupiravir
ORF1a: G209S			
ORF1a: V2130I			
ORF1b: R1729H			
ORF3a:M1I			
ORF3a: G224S			
S: S247R			
S: V483I			

660 **Supplementary Figures**

661 **Figure S1**

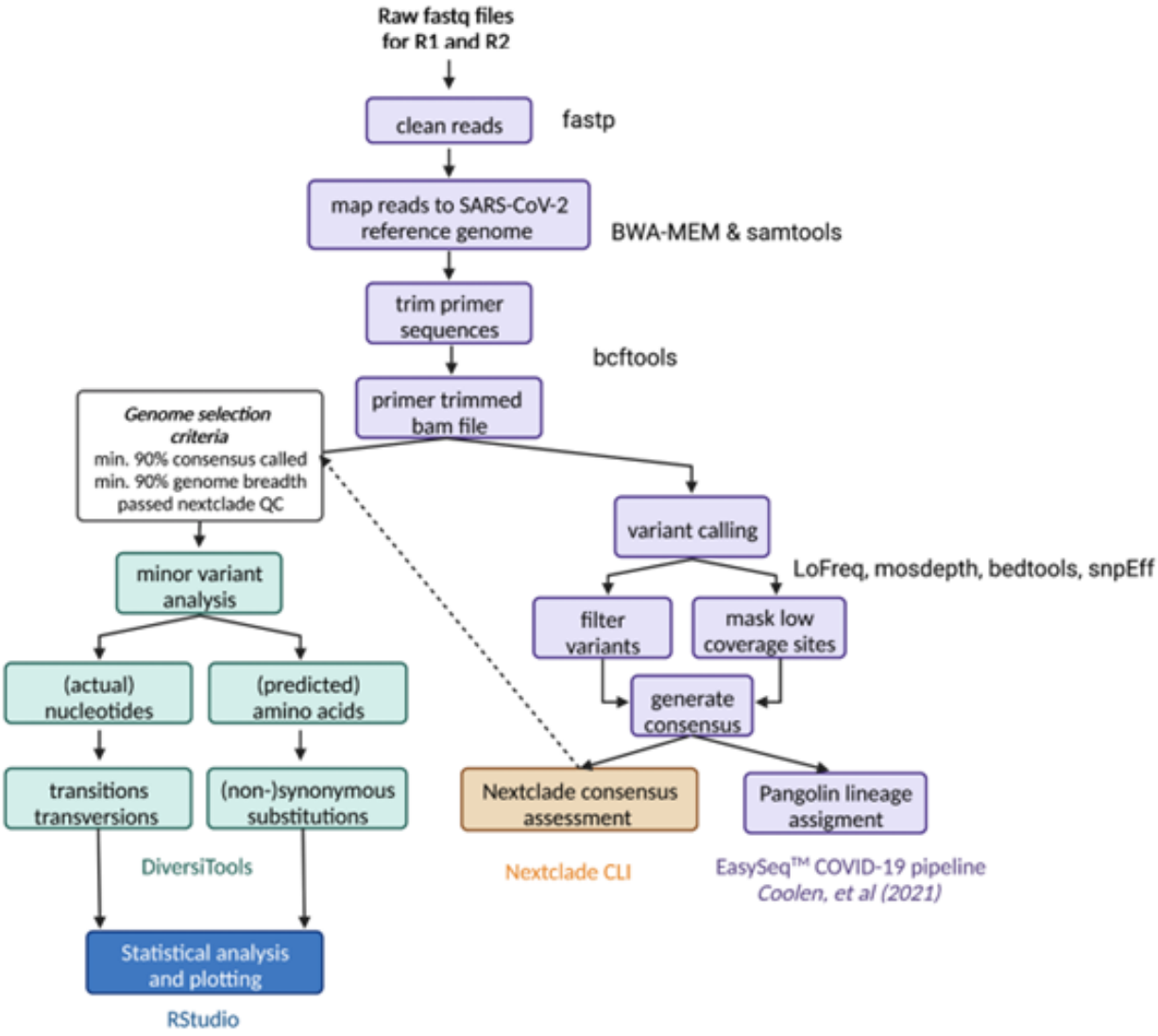

662

663 Bioinformatic workflow used for sequencing analysis.

Figure S2

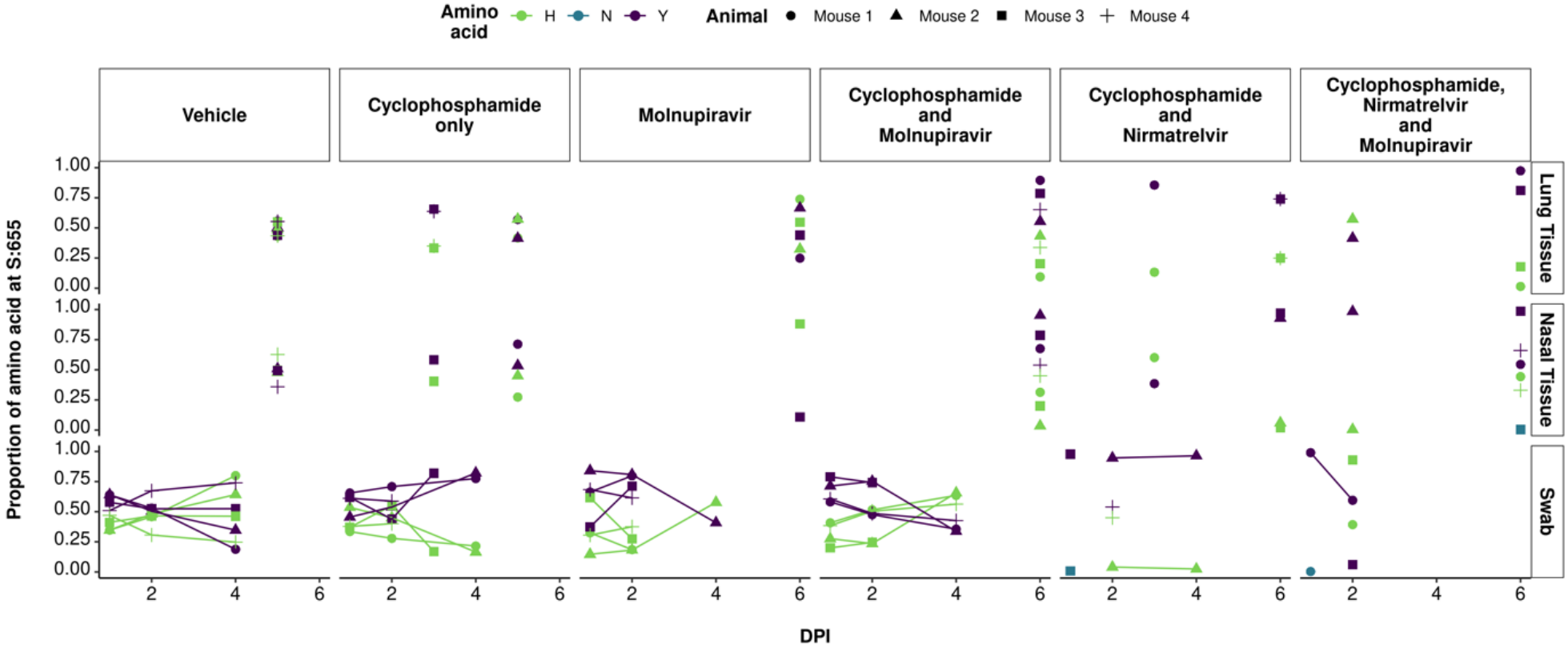

The proportion of amino acid H and Y at position 655 in the Spike protein over time or in lung or nasal tissues. The S: H655Y mutation was observed at the minor variant level if not observed in the consensus level. Each point represents one animal within the cohort.